EPJ manuscript No.
(will be inserted by the editor)

Electric Birefringence Study of an Amyloid Fibril System: the Short End of the Length Distribution

Salman S. Rogers[1], Paul Venema[2], Jacques P. M. van der Ploeg[3], Leonard M. C. Sagis[2], Athene M. Donald[1], and Erik van der Linden[2]

[1] Department of Physics, Cambridge University, Cavendish Laboratory, Cambridge, CB3 0HE, UK
[2] Laboratory of Food Physics, Wageningen University, P.O. Box 8129, 6700 EV Wageningen, The Netherlands
[3] Leiden Institute of Chemistry, Leiden University, P.O. Box 9502, 2300 RA Leiden, The Netherlands

Revised: 18 July 2005

Abstract. In this article, a system of amyloid fibrils, based on the protein β-lactoglobulin, is studied by transient electric birefringence. Single pulses of an electric field were applied to the solution, and the initial rise and subsequent decay of birefringence analysed. The decay takes place on a range of relaxation times, and therefore contains information about the length distribution of fibrils in the system. The information can be extracted using theories of the electric polarisability of polyelectrolyte rods, since the fibrils are an example of these. Despite the long-standing complications of such theories, useful quantitative information about the system can still be obtained. Using the Fixman model of polyelectrolyte polarisability, we obtain a measurement of the short end of the length distribution which shows the fibril concentration as a function of length rising linearly from 0.02–2μm. The short end of the length distribution was unobtainable in our previous study using rheo-optics (Rogers S. S. et al., Macromolecules **38**, 2948 (2005), Iss. 8), but reasonable agreement between the two techniques shows they are complementary.

PACS. 82.35.Pq Biopolymers, biopolymerization – 82.35.Rs Polyelectrolytes – 83.85.Ns Data analysis – 87.14.Ee Proteins – 87.15.Nn Properties of solutions; aggregation and crystallization of macromolecules – 87.15.Vv Diffusion

1 Introduction

Various proteins are known to misfold and aggregate in mildly denaturing conditions, into rod-like structures known as amyloid fibrils. Some of these systems are interesting medically, being associated with various degenerative diseases [1–4]. Others may find useful application in food or biomaterials [5,6]. The structures involved are also interesting from the more fundamental viewpoint of protein physical chemistry [7]. Thus, considerable work has been dedicated to these systems over recent years, and aspects of their structure and formation have been studied by a range of techniques [8,9].

One characteristic of these systems, about which relatively little is known, is their length distribution. Knowledge of this would provide a means to test the various candidate models of fibril assembly kinetics, which otherwise remain largely qualitative and speculative [10]. Moreover, it would provide significant information on the potential utility of these fibrils in a biomaterial or food gel, since the mechanical properties would crucially depend on length, just as for traditional polymer systems [11].

Techniques for measuring particle sizes or lengths are similarly important in the study of other systems of particles in solution. Electro-optics has been applied for this purpose before [12,13] since its utility in measuring relaxation of many systems is well established. It has previously been applied to systems of rod-like particles in aqueous solution such as: DNA fragments [14], filamentous viruses [12,15], and rod-like colloids of latex [16], gold [17] and clay [18]. For a monodisperse fibril system, only a theory linking rotational diffusion to length is required to extract a length from the relaxation of birefringence or dichroism. However, new and unresolved complications arise in studying a polydisperse fibril system with electro-optics, which we address in this article. Importantly, a theory of electric polarisability as a function of length is required for a detailed quantitative analysis.

In our previous article [19], we studied the length distribution of amyloid fibrils based on bovine β-lactoglobulin (β-lg), by applying rheo-optics: using a macroscopic optical measurement of the solution under flow as a probe of its microscopic dynamics. In the present article, we present complementary results and analysis on an identically prepared system, but using electric rather than flow fields

Correspondence to:
E. van der Linden, e-mail: erik.vanderlinden@wur.nl,
or Athene M. Donald, e-mail: amd3@phy.cam.ac.uk

to align the fibrils. β-lg solutions form amyloid fibrils under prolonged heating at low pH and low ionic strength [20,21]. These fibrils are polydisperse in length (with an average length of the order of 1μm) and monodisperse in cross-section, with a width of about 4nm [20,22]. The persistence length, is approximately 1.6μm — of the same order of magnitude as the length [23]. At conditions of pH2, 5mg/ml concentration, no added salt and heating at 80°C, transparent solutions of fibrils are produced without macroscopic aggregates [23,24]. The fibrils show a twisted strand structure, one or two protein monomers across in cross-section [22,24]. The line density of molecules in the fibril (i.e. molecules per unit length) is 0.28nm^{-1} according to neutron scattering measurements [24].

Far from the isoelectric point, β-lg fibrils, like many other biopolymers, have a high electric polarisability. This is understood to be due to the counterion cloud which surrounds each fibril and moves in response to an electric field. With an ionic charge of around +21 per molecule at pH2 [24,25], and hundreds or thousands of molecules per fibril, β-lg gives a good example of this effect. Describing the polarisability of these 'polyelectrolyte' rods is a fundamental but formidably difficult problem, and has been studied theoretically [26–32], and experimentally [14,31, 33,34] over the past 45 years.

In this article, we apply two different theories of the polarisability of rod-like polyelectrolytes, the sophisticated theory of Fixman [29] and the more archaic theory of Mandel-Manning [28], to our measurements. These theories are well known, but also attractive because of their lack of arbitrary parameters. From each, a very different length distribution is extracted from the measurements, but only the outcome of the Fixman theory is consistent with previous results. Using this theory, some useful and quantitative information is extracted about the short end of the fibril length distribution, which was inaccessible using rheo-optics [19].

2 Experimental Section

2.1 β-lg fibril preparation

All experiments were performed on bovine β-lg obtained from Sigma (L-0130-5G, batch 033K7003, a mixture of genetic variants A and B). The protein was dissolved in dilute hydrochloric acid at pH2, and extensively dialysed with the same pH2 hydrochloric acid to remove traces of calcium ions and obtain a solution with the same ionic strength as the solvent. The solution was centrifuged at 22600g for 30 min and filtered through a 0.45μm filter to remove aggregates and undissolved protein. A UV spectrophotometer was used to measure the concentration of this stock solution, using a calibration curve from known β-lg concentrations, determined at a wavelength of 278nm. The stock solution was used to make a 15ml sample which was made up to 5mg/ml concentration, in pH2 HCl with no added salt. It was heated in a glass vessel for 24 hrs at 80°C using a water bath, during which it was stirred constantly with a magnetic stirrer. Sodium azide (200ppm) was added to the resulting fibril solution to prohibit microbial growth, and the solution refrigerated at 4°C before measurements were made. This preparation is identical to that used previously for the rheo-optics study [19].

2.2 Electro-optical experiments

Transient electric birefringence experiments were performed with a conventional setup [18] as follows: light from an 8mW helium-neon laser (632.8nm wavelength) travels through a high-quality Glen Thompson polariser. This polariser is oriented in such a way that linearly polarised light is obtained with its axis of polarisation at $\pi/4$ with respect to the electric field, while its axis of propagation is perpendicular to the field. After passing through a cell containing the solution, the beam travels first through a polariser (analyser) before its intensity is converted to a voltage by a photomultiplier tube. The presence of a quarter-wave device increases the sensitivity and makes it possible to distinguish the sign of the birefringence. The voltage of this tube and the voltage applied on the solution are measured simultaneously by a digital oscilloscope (LeCroy 9450). The voltage of the tube is calibrated to obtain the birefringence signal $\Delta n(t)$. The solution is contained in a quartz cuvette with two parallel, rectangular platinum electrodes. The electrodes are held apart at a fixed distance of 1.89mm. The optical path length is 49.05mm, the length of the electrodes. The temperature is kept constant at 21°C by circulating water from a thermostated bath through a jacket which holds the cell. The voltage to be applied across the electrodes is supplied by a function generator (WaveTek 29) in combination with a high-speed power amplifier (NF Electronic Instruments 4020, Bandwidth 500KHz, max 250V) or a very high speed pulse generator (Cober Model 606, rise/fall time $<$ 100ns, max 2500V). In this way, single pulses of variable voltage and time were generated. The response time of this setup is better than 1μs. Computer control of the function generator and oscilloscope allows pulses to be repeated and averaged, leaving a lag time for the system to relax between pulses. This lag time is judged to be long enough when the optical response to successive pulses stays the same, within the noise of measurement.

The fibril solution, as prepared above, was diluted 20–200 times in distilled water or low concentration HCl before electro-optical measurements were made. This was necessary to reduce the ionic conductivity and relaxation time of the system, thereby allowing shorter duration pulses of higher fields to be used, while avoiding the effects of heating and electrode reactions. It was not possible to reach steady birefringence, even with these dilutions under weak fields. Applying longer duration pulses resulted in a noticeable artifact due to sample heating, before any steady state could be reached. (This artifact consists of a negative contribution to the birefringence, due to the density change caused by uneven heating — an analogous effect to an atmospheric mirage.) Therefore, we measured the opposite extreme: short pulses of the field, during which the birefringence was still very far from the steady

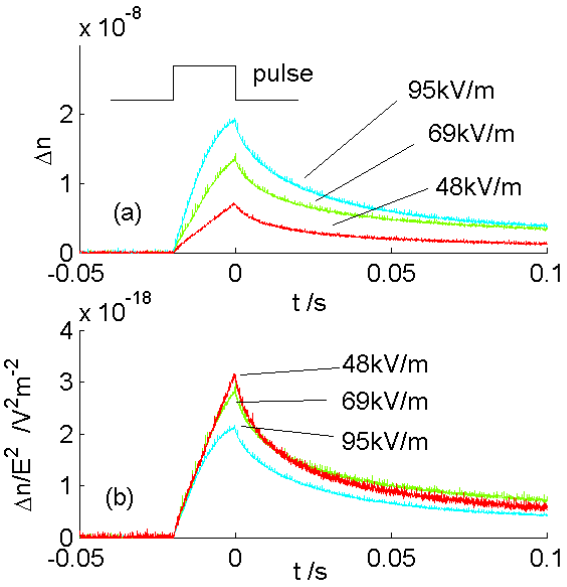

Fig. 1. Birefringence response (a) from 20ms pulses across the fibril solution, at $\nu = 50$, with various field strengths. These are divided by E^2 in (b), showing the scaling of the initial rise gradient.

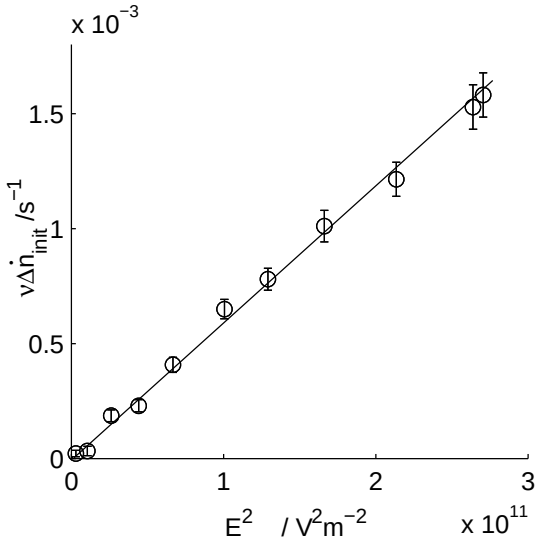

Fig. 2. Dependence of the initial birefringence rise gradient $\Delta\dot{n}_{\rm init}$, on field, for the solution at $\nu = 50$, showing the dependence $\Delta\dot{n}_{\rm init} \propto E^2$.

state. This is an apparently novel development of the transient electric birefringence technique.

3 Results

Fig. 1a shows measurements of the birefringence response from pulses of field $E = 48$–$95\mathrm{kVm}^{-1}$ for duration $\Delta t =$ 20ms, on a sample of the prepared fibril solution diluted 50 times in water (dilution $\nu = 50$). This dilution takes it to a pH of 3.7. Sixteen consecutive pulses were averaged to give each signal, with a delay of 45s between pulses to allow the system to equilibrate. It was found that the system did not degrade under any of the combinations of E and Δt present in this article, since within the noise of measurement, the response did not change after successive pulses. The graph shows an increase in birefringence with time during the pulse, this increase being nearly linear at early times, and followed by a slow decay. The standard interpretation of this signal, in terms of initial orientation of the fibrils followed by subsequent orientational decay, is due to Benoît [35,36] and O'Konski & Zimm [37], and is detailed in Appendix A.

It is clear from this graph that the diffusion of the system is far too slow to allow us to reach a steady state of birefringence for pulses of this duration, even at this dilution. However, averaging the signals from consecutive pulses, as we have done, reduces the noise sufficiently so that the initial gradient of birefringence increase at the start of the pulse can be determined and analysed. As detailed in Appendix A, this 'rise gradient', $\Delta\dot{n}_{\rm init}$, depends on the polarisability $\Delta\alpha$, length concentration c_L and rotational diffusivity D_r of the fibrils, each as a function of fibril length, as well as the field strength E. (Note c_L is the number of fibrils, per unit volume, times their length.) We therefore begin by examining the dependence of $\Delta\dot{n}_{\rm init}$ on E and ν to check the applicability of Benoît's interpretation, which predicts (see Appendix A):

$$\Delta\dot{n}_{\rm init} = \frac{2ME^2}{k_BT}\int_0^\infty c_L\Delta\alpha D_r dL\,, \qquad (1)$$

where k_B is Boltzman's constant, T is the absolute temperature, and M, the optical anisotropy per unit length concentration, is $1.74\times10^{-20}\mathrm{m}^2$ (determined in our previous study, Ref. [19]). It must be stressed that this value of M, which depends on a measurement of the total conversion of β-lg monomers to fibrils, is of questionable accuracy [19]. However, by using the same value of M as in our previous study, our results for the length distribution (which are proportional to $1/M$) should still be mutually consistent, even if they deviate from the absolute value by some factor. Note that in Eq. 1, the initial rise of birefringence is independent of any permanent dipole moment which the fibrils might have. This is explained in Appendix A.

Fig. 2 shows the dependence of the initial rise on the field strength, again in a sample of $\nu = 50$, diluted in water. Voltages of up to 1000V were applied across the electrodes. $\Delta\dot{n}_{\rm init}$ is proportional to E^2 in the full range of field strengths, as predicted by Eq. 1, which is analogous to the Kerr law [33]. (Likewise, in Fig. 1b, the measurements of Fig. 1a are divided by E^2, which scales them onto a single straight line at early times, after which they deviate.)

Next we investigated the dependence of the initial rise on concentration ($1/\nu$), as shown in Fig. 3, where for each ν in the range 20–200, the prepared solution was diluted by a factor of ν in water or dilute hydrochloric acid so that the final concentration of HCl was made up to 0.5mM.

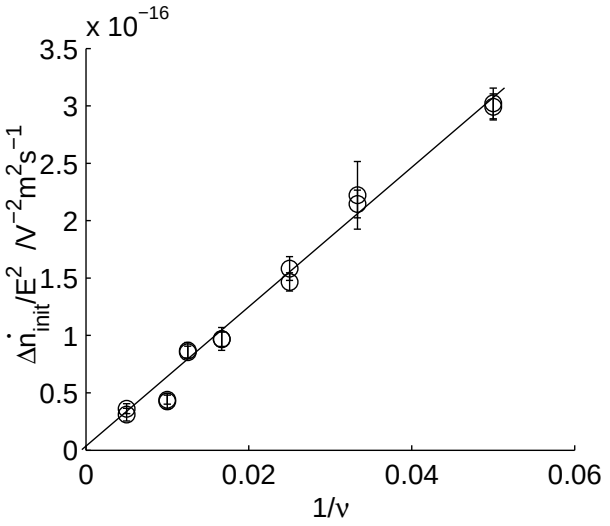

Fig. 3. Dependence of the rise gradient $\Delta\dot{n}_{\rm init}$, on concentration, for the solution diluted in the range $20 \leq \nu \leq 200$. $\Delta\dot{n}_{\rm init}/E^2 \propto 1/\nu$, indicative of the dilute diffusion regime.

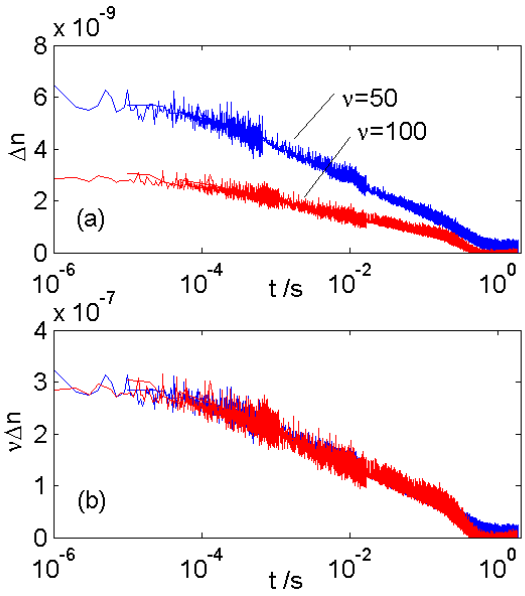

Fig. 4. Birefringence decays (a) from 240μs pulses of $E = 423{\rm kVm}^{-1}$, at $\nu = 50$ and $\nu = 100$, both at [HCl]=0.2mM. Measurements at different sampling rates have been overlaid. In (b) the curves are scaled by concentration, showing good agreement and complementing the concentration dependence of Fig. 3.

This was done so that the ionic conditions would be constant at all concentrations, thus keeping polarisability constant for each fibril. Within the noise of measurement, a linear dependence of $\Delta\dot{n}_{\rm init}/E^2$ on $1/\nu$ is maintained over the full range of concentration. Since the fibrils are undamaged by dilution, as found previously [19], the length concentration c_L of the system scales with dilution as:

$$c_L \rightarrow c_L/\nu\,. \qquad (2)$$

Because of this scaling, Eq. 1 predicts that $\Delta\dot{n}_{\rm init}$ has at least a linear dependence on $1/\nu$, due to the c_L factor, as well as any implicit dependence on D_r. Such an implicit dependence will occur if D_r varies with concentration due to entanglement effects. In Fig. 3 we observe only a linear dependence, and therefore conclude that D_r is constant with respect to concentration. This point will be discussed in Section 4.1.

Benôit's model gives us a standpoint with which to study the length distribution, at least at its short end, as we will discuss. After the pulse, the birefringence decays on a spectrum of relaxation times, since the diffusion of long rods is slower than that of short rods. The resulting decay curve can be analysed to extract the length distribution of the fibrils, within limitations set by measurement noise and the assumptions necessary in describing their behaviour (Section 4). Birefringence decays are shown in Fig. 4a for the sample diluted to $\nu = 50$ and $\nu = 100$ in water, with the HCl concentration of the latter made up to 0.2mM so that the ionic conditions would match the former, and only the fibril concentration would vary between them. Pulses of $E = 423{\rm kVm}^{-1}$ (800V across the electrodes) and $\Delta t = 240\mu$s were applied. We chose a large field so that the pulse duration could be made as small as possible, to ensure that the alignment during the pulse remains far from a steady state for as wide a range of lengths as possible in the system (see Appendix A). Making the pulse short has the effect of reducing, as much as possible, the effect of any permanent dipole moment which the fibrils might have, thus simplifying our analysis in the next section.

In Fig. 4a, each line comprises three collected at different sampling rates, each the mean of 32 consecutive measurements, with delays of 60s between pulses. In Fig. 4b, these decays are scaled by concentration. A remarkably good superposition is seen, in agreement with the concentration dependence we observed in Fig. 3, except for a slight deviation at the long-time end of the decays, on which we comment in the following section.

The two scaled decays of Fig. 4b are averaged into a master decay, and resampled onto 100 logarithmically sampled points of time. Logarithmic resampling is most appropriate since it can adequately describe the decay, which takes place across 6 orders of magnitude of time. Next, we take a discrete inverse Laplace transform of this master decay (Fig. 5), to obtain the spectrum of decay times present in the system's response, corresponding to a range of fibril lengths. 8 discrete components of the birefringence G_j (where $j = 1, 2...8$), are taken, sampled logarithmically with decay time τ. After taking an initial estimate, $\{G_j\}$ is adjusted until the decay curve calculated from it converges with the measured decay curve (see Appendix B). This kind of fitting procedure can produce ambiguous results, so we must check how robust it is. By varying our initial estimate, we check whether the same distribution $\{G_j\}$ is obtained. As seen in Fig. 5, a smooth distribution of $\{G_j\}$ is obtained with fairly low variation between the fits from different initial estimates, showing

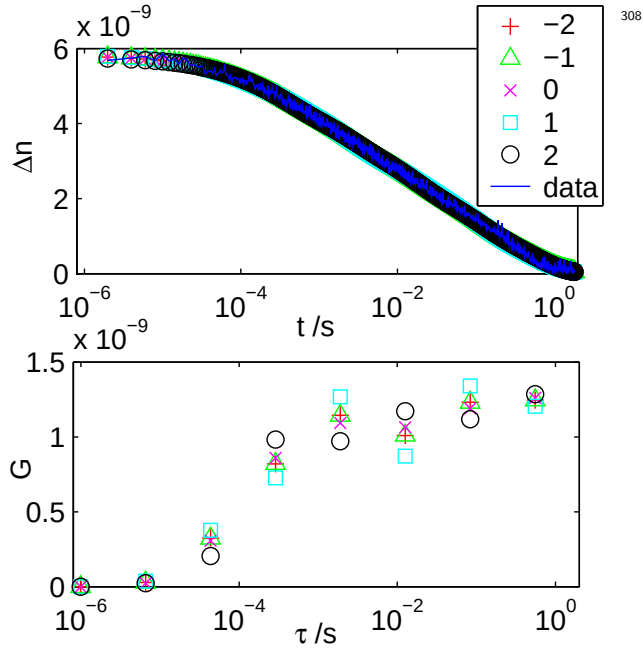

Fig. 5. Discrete inverse Laplace transform of the mean of the decays in Fig. 4. Discrete components of the birefringence G_j are taken, logarithmically sampled in decay time, τ. The components are adjusted from initial estimates in both directions of τ (labelled -2, -1, 0 1, 2) to provide an estimate of fitting error due to noise (see Appendix B).

that the fit is robust. The mean and maximum deviation of each G_j in these fits are used to give an estimate of the ambiguity of fitting due to noise. The maximum deviations are used in all following figures to plot error bars due to noise.

4 Data Analysis

4.1 Measured birefringence as a function of length

In the previous section, we found that the initial rise gradient of birefringence had a linear dependence on $1/\nu$, which shows D_r is constant with respect to concentration. This result is, at first, surprising. In our previous study on the rheo-optics of an identically prepared system [19], we found that the diffusivity of the fibrils was proportional to ν^2, in the way predicted by Doi and Edwards [38] for rods which overlap and hinder each other's motion (the semidilute regime). By contrast, we find here that the diffusivity is independent of concentration, for the same system. The only simple explanation for this is that under the electric field, we are preferentially orienting and observing the short end of the length distribution: the fibrils which are short compared to the entanglement length [19]:

$$L^* = \left(\int_0^\infty c_L dL \right)^{-1/2} . \qquad (3)$$

For this system $L^* = 52\text{nm} \times \sqrt{\nu}$ as determined previously [19]. In the case of $\nu = 50$, $L^* = 0.37\mu$m. We therefore argue that the birefringence response to the electric field is dominated by fibrils below this length, and therefore in the dilute diffusion regime [39]. The consistency of this picture will be verified below, and explained in terms of diffusivity and polarisability.

Fibril lengths corresponding to the different decay times in Fig. 5 may be calculated using the well known diffusivity of thin rigid rods of length L in the dilute regime:

$$D_r = \frac{k_B T}{3\pi\eta L^3} \ln(L/d) . \qquad (4)$$

This diffusivity was originally calculated by Kirkwood et al. [40,41], developed by Broersma [42] and Tirado & Garcia de la Torre [43] for end effects, reviewed by Tracy & Pecora [39] and experimentally verified for many systems of stiff polymers in dilute solution, (see e.g. Ref. [14].) The relation has a slight dependence on diameter d, which we take as 4nm [22]. Using Eq. 4, the discrete contributions to the birefringence decay, $\{G_j\}$ can be recalculated into the form of a continuous distribution g, according to Eq. 24 (Appendix B). Fig. 6 shows the result. This distribution of contributions to the decay g, is a weighted version of the length distribution $c_L(L)$:

$$g = c_L S(L, \Delta t) , \qquad (5)$$

where $S(L, \Delta t)$ is the alignment parameter for fibrils of length L at the end of the electric field pulse. We must calculate $S(L, \Delta t)$ in order to find c_L. As can be seen in Fig. 6, the peak of the weighted distribution g is below the entanglement length $L^* = 0.37\mu$m calculated above, and confirms that our earlier hypothesis is consistent: that the electric field is preferentially aligning the short end of the length distribution within the dilute regime. At lengths somewhat higher than L^*, we expect the diffusivity to rapidly decrease with length, as the rods enter the semidilute regime and become entangled. Hence the alignment during the pulse, $S(L, \Delta t)$ would also decrease rapidly, since it is approximately proportional to D_r (see Appendix A). It is likely that the slight discrepancy at the long-time end of the superposed decay curves in Fig. 4b, as noted above, is caused by the slight alignment of fibrils at the 'edge' of entanglement. Pecora et al. [44,45] found the onset of entanglement to occur at about $4L^*$.

This idea may be compared with our measurements. Fig. 6 has an upper cut-off at $L = 1.9\mu$m, which has come about because no components of relaxation time greater than 0.55s were required to fit the decay curve in Fig. 5. In other words, no alignment of fibrils of length much greater than 1.9μm was detected within the noise of measurement, and the distribution of contributions to the decay (Fig. 6) drops abruptly to zero, somewhere between $L = 1.9\mu$m and $L = 3.5\mu$m where the next exponentially sampled point was due. Since previous results have shown the c_L is still far from zero in this range, this is likely to be due to the onset of semidilute behaviour. In terms of entanglement length, 1.9μm–3.5μm is the range $5.2L^*$–$9.5L^*$,

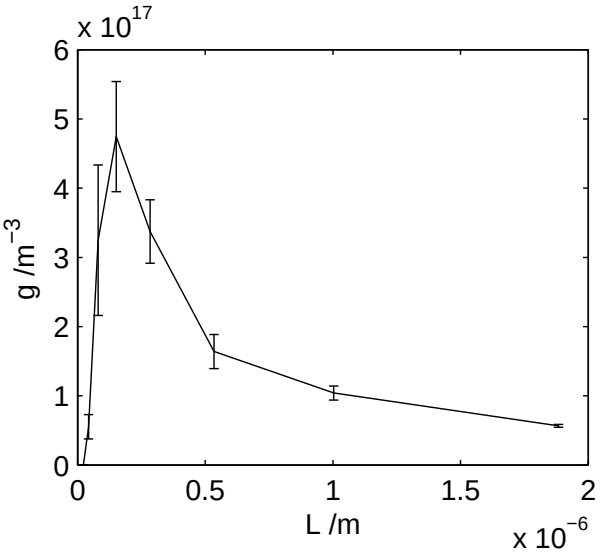

Fig. 6. Plot of g, the distribution of contributions to the master decay curve, as a function of L, where Eq. 4 has been used to relate decay times with L.

which agrees approximately with the results of Pecora et al.

4.2 Polarisability of polyelectrolyte rods

An important piece of information necessary to calculate $S(L, \Delta t)$ is $\Delta\alpha$, the electric polarisability anisotropy of the fibril, which we model as a polyelectrolyte rod. This has been studied theoretically by a range of authors, (recent reviews in Refs. [31,32]) yet it remains a formidable theoretical problem. Early studies considered only the contribution of 'bound' counterions, which remain close to the surface of the polyelectrolyte rod because of electrostatic attraction, but are free to move along the length of the rod. This freedom of movement leads to a polarisability which is large for such systems and thought to be the major contribution to $\Delta\alpha$. Mandel provided the prototypical model [26], which was successively developed by Oosawa [27] and Manning [28]. The latter predicts:

$$\Delta\alpha^{(\mathrm{Manning})} = \frac{\phi z^2 e^2 L^3}{12 k_B T b}[1 - (2|z|Qb^{-1} - 1)\ln\kappa b]^{-1}\,, \quad (6)$$

where z is the counterion valency, e is the electronic charge, b is the mean spacing of charges on the polyion, $Q = e^2/4\pi\epsilon\epsilon_0 k_B T$ is the Bjerrum length, κ^{-1} is the Debye length, where

$$\kappa^2 = \frac{2I \times 10^3 N_A e^2}{\epsilon\epsilon_0 k_B T}\,, \quad (7)$$

I is the molar ionic strength (of small ions), N_A is Avogadro's number, ϕ is the fraction of counterions bound to the polyion as calculated by Manning's condensation theory [28]:

$$\phi = 1 - \frac{b}{Q}\,, \quad (8)$$

and the relative permittivity of water, $\epsilon = 80.1$. Manning's theory, like all the related theories, predicts $\Delta\alpha$ to be proportional to L^3.

Fixman [29] took a more sophisticated approach to the problem, considering also the electric field of the counter- and co-ions and their flux through the double layer surrounding the cylindrical polyion, which were ignored by the previous theories. The main qualitative change from the earlier theories is that the flux of ions leads to a screening of the induced dipole at longer rod lengths. Thus, $\Delta\alpha^{(\mathrm{Fixman})}$ has an L^3 dependence at small L which gradually changes to a linear L dependence at large L, and is given by:

$$\Delta\alpha^{(\mathrm{Fixman})} = \frac{4\pi\epsilon\epsilon_0 L K z_1}{\gamma^2(z_1 - z_2)}\left(1 - \frac{\tanh(\gamma L/2)}{\gamma L/2}\right)\,, \quad (9)$$

where z_1 and z_2 are the valencies of the counter- and co-ions, γ^{-1} is the characteristic 'screening length' given by:

$$\gamma^2 = \frac{4\pi c_1 K b}{\phi}\,, \quad (10)$$

c_1 is the bulk concentration of counterions and K is a numerical factor given by:

$$K = (2\ln(2L/d) - 14/3)^{-1}\,. \quad (11)$$

The fraction of bound counterions, ϕ, is given by the Manning condensation theory as above. Several authors [31,30,46] consider the Fixman theory to be the most useful model of rod-like polyelectrolyte electric polarisation. Other models have been published, based on similar physics and reaching similar results, and applying to particles with various geometries. Most are discussed in Ref. [31] or stem from work reviewed therein.

The Manning and Fixman theories have been compared with experimental results for DNA fragments by Elias & Eden [14], and polystyrene-sulphonate chains by Tricot & Houssier [34], each using various lengths. The two studies confirm an L^3 dependence of polarisability at small L, which decreases to an approximately linear dependence at large L, although the data at large L was limited. The absolute values predicted by both theories were found to give useful, though not accurate, values approximately within a factor of 2 of the experimental results.

In Fixman's derivation, it was assumed that the diameter of the polyion is large compared to the double layer of counterions around it. In our case, at $I = 0.4$mM, $\kappa^{-1} = 15$nm compared to $d = 4$nm. This value of κ^{-1} is similar to those of both of the experimental studies mentioned above, but here d is larger by a factor of about 2 (compared to DNA and polystyrene-sulphonate). Therefore, while the assumption may be regarded as crude for our system, it is in fact similar or at least as good as in the previous studies.

I	0.4mM
b	$1/(7.9 \times 0.28\text{nm}^{-1}) = 0.45\text{nm}$
κ^{-1}	15nm
ϕ	0.35

Table 1. Electrostatic parameters for the fibril solution at $\nu = 50$

When diluted to $\nu = 50$ in water, the pH of our prepared fibril solution becomes 3.7. In order to calculate b, we need a value of the net charge per monomer, for which we take $+7.9\pm0.5$ at pH3.7 [1]. $\Delta\alpha$ is rather sensitive to the charge according to both theories, so it is appropriate to take this measured value rather than the commonly used 'ideal' value, which equals the sum of charges of each isolated residue as a function of pH [47]. (For β-lg, the 'ideal' charge is +15.9 at pH3.7.) We have calculated the relevant parameters for both theories, for our system at pH3.7. The results are shown in Table 1.

4.3 Extracting the length distribution

Using the polarisability of the Fixman and Manning theories, $S(L, \Delta t)$ is calculated numerically according to Benoît's model (Appendix A). One additional parameter must be considered, and this is the permanent electric dipole moment of the fibril μ, as yet unknown. Since the fibril has a net charge, formally we should describe this moment as the first moment of the charge distribution around the rotational centre of drag [48]. However, because it is commonly referred to as the dipole moment, and is more easily referred to and visualised as such, we will also refer to it as the dipole moment. For μ, we will model a linear dependence on the fibril length:

$$\mu = \mu' L \,. \tag{12}$$

where μ' is then the dipole moment per unit length. This is a reasonable approach because the fibril is a chain of monomers, and therefore the charge distribution of the whole fibril is the sum of the charge distributions of the monomers. If there is any order in the arrangement of monomers in the fibril, we would expect a dipole moment of this form. (If there is no order in the arrangement of monomers, we would expect a dipole moment of zero.) μ' is then the only free parameter in the calculation — the others are controlled directly, or modelled by the theories of polarisability and diffusion.

We can see how this uncertainty in μ' affects the length distribution by calculating $S(L, \Delta t)$ with various values of μ'. The results are shown in Fig. 7 according to the Fixman theory. A realistic estimate for the upper limit to μ' is the ratio between the monomer's dipole moment and its diameter, so that the dipole moment of the fibril is the sum of the moments of its monomers oriented 'head-to-tail'. The dipole moment of the β-lg molecule has been studied by dielectric measurements [49], yielding a value of 730D, which compares well with a calculation of the dipole moment of 625D according to the X-ray crystal structure [50]. (In S.I. units, $1\text{D} = 3.3\times10^{-30}\text{Cm}$). Taking the radius of gyration as 1.7nm [50] allows us to estimate that μ' lies in the range $0\text{–}7\times10^{-19}$C. In the corresponding calculations of c_L (Fig. 7), it can be seen that this range causes an ambiguity which is significant below about $L = 0.5\mu$m, but negligible for larger lengths, i.e. lengths corresponding to relaxation times longer than Δt. We see therefore, that making Δt as small as possible, as we have done, reduces the permanent dipole moment from being an important parameter to being a modest source of quantifiable error. We will investigate the permanent dipole moment in more detail in a forthcoming article.

In Fig. 8, the predictions of c_L using the Fixman and Mandel-Manning theories are compared, with error bars due to fitting error and uncertainty in μ'.

Using the Fixman theory, c_L increases steadily with L in the range 0.02–1.9μm. By contrast, the Manning theory predicts a peak at around $L = 200$nm, and steadily decreasing c_L thereafter. This large qualitative difference between them is due to the significant disagreement between the theories at $L > 1/\gamma$, i.e. $L > 34$nm in our system. The alignment $S(L, \Delta t)$, is approximately proportional to $D_r\Delta\alpha$ in Benôit's model (see Appendix A). Therefore $S(L, \Delta t) \propto L^{-2}$ according to the Fixman theory, which predicts $\Delta\alpha \propto L$ in this range, but $S(L, \Delta t)$ is constant according to the Manning theory, which predicts $\Delta\alpha \propto L^3$. Comparing the two predictions with our previous results on the system, using rheo-optics and TEM, which show a peak at around 5μm [19], it can be seen that only the one using Fixman's theory is consistent with the previous results. In terms of absolute value, the c_L according to Fixman is approximately twice the previous results, while according to Manning, it is a factor of 10 too small.

In Fig. 9, the length distribution according to the Fixman theory is divided by 2.5 to match it with the length distribution according to rheo-optics/TEM. The gradients match very well.

5 Discussion

Our method has predicted c_L for L below 1.9μm. Using Fixman's polarisability model, c_L compares favourably with previous results [19] except for a difference in absolute value — a factor of 2.5. If we are to consider the absolute value of the previous results to be correct, this means that Fixman's $\Delta\alpha$ has the correct dependence on L, but is too small by a factor of about 2.5. Other experimental studies of Fixman's theory [14,34] also came to this conclusion, and it is possible that the difference is due to the contribution of free counterions to the polarisability [34]. Alternatively it may be due to the crudeness of our thin double layer approximation, in common with these other studies. It is also worth noting that the absolute value is proportional to the fraction of bound counterions ϕ, which

[1] The ionisation of β-lg as a function of pH was measured by titration in Ref. [25], and is quoted as the charge per 40kDa, the approximate mass of a dimer. We have recalculated the charge according to the monomer mass of 18.6kDa.

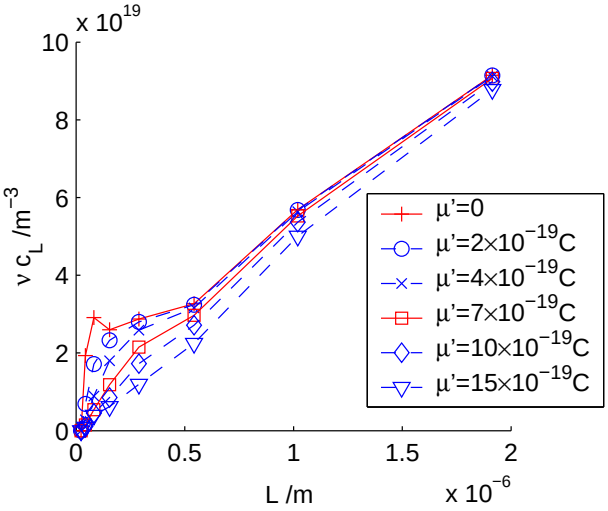

Fig. 7. Length distributions of fibrils in the sample, calculated using the Fixman model of polarisability for various values of the permanent dipole moment per unit length μ'.

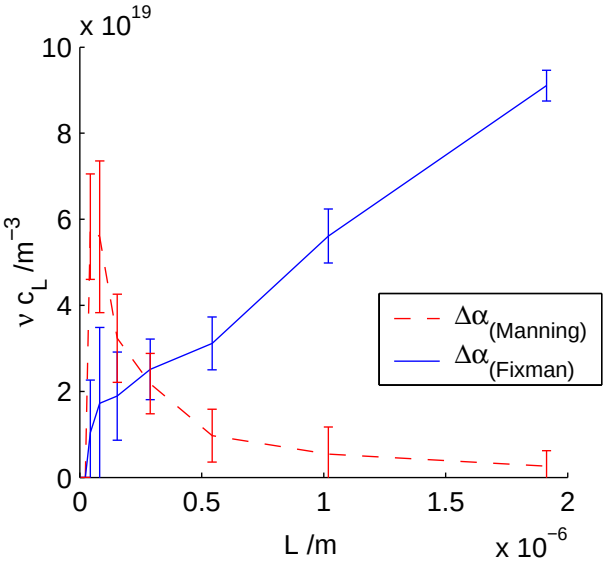

Fig. 8. Length distributions of fibrils in the sample, calculated using the Fixman and Mandel-Manning models of polarisability. The distributions differ considerably: only the Fixman model leads to a result complementary to previous results [19].

depends sensitively on the charge of the monomer and the line density.

The present result complements those of the rheo-optical method on the same system [19] and shows that the Fixman theory describes the polarisation of the system better than the archaic Mandel-Manning theory. In previous studies on other systems mentioned above [14,34], measurements of polarisability as a function of L showed a transition from a cubic to an approximately linear dependence on L, which is only predicted by the Fixman theory. Therefore, it may generally be the case that the Fixman

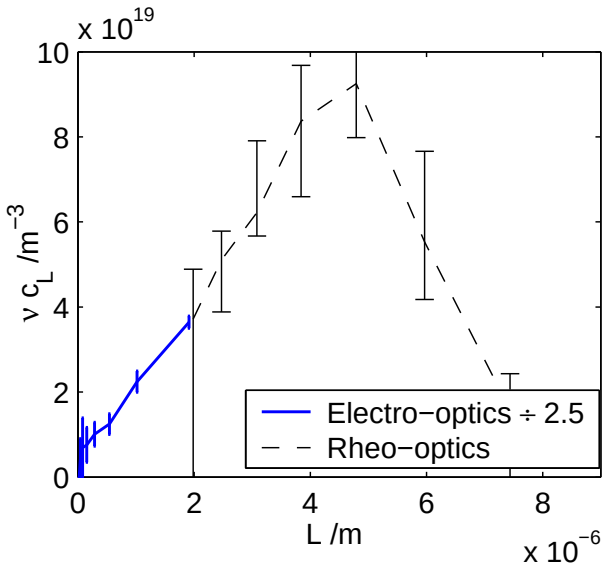

Fig. 9. Length distribution of fibrils in the sample according to the present electro-optical method using the Fixman theory compared with the previous rheo-optical method [19]. The former has been divided by 2.5 so that their absolute values match.

theory describes the polarisation of long polyelectrolyte rods better than the Mandel-Manning theory.

It is interesting to compare our two relaxation methods, based on rheo- and electro-optics, as applied to the same system. The rheo-optical method was able to measure undiluted samples; flow was applied in order to align the fibrils completely, which led to complications due to their stretching. The main experimental limitation in that case was the finite time taken for the flow to stop, forbidding the measurement of the shorter relaxation times, and therefore the short end of the distribution. The present electro-optical method required diluted samples in order to reduce the ionic conductivity; short pulses of an electric field were applied to align the fibrils, which led to a complication due to modelling the polarisability as a function of length. The main experimental limitation was the finite duration of the pulse, which leads to errors in the analysis of shorter relaxation times. The rheo-optical method was able to measure the long end of the length distribution, and the electro-optical method has been able to measure the short end.

Considering the short end of the length distribution (according to Fixman's theory), one striking observation is made. The length distribution starts at or near zero length concentration from $L = 0.02\mu$m and increases linearly, within the error bars. Other authors, working on the β-lg system [22,51], and on other amyloid fibril systems [52,53] have written about the possible or observed formation of other species of protein aggregates, intermediate in size between fibrils and monomers. If such intermediates were present and rod-like in shape, we would expect to see a peak in Fig. 9, if they were present in the system in appreciable quantities compared to the fibrils. However,

there is no sign of any such peak in the measured range of the length distribution.

6 Conclusion

Using the technique of transient electric birefringence, we have investigated β-lactoglobulin fibrils, a highly polydisperse rod-like system. Interpretation of the results according to Benôit's model [36], and Fixman's theory of polarisability of polyelectrolyte rods [29], yields a measurement of the short end of the length distribution. This short end distribution complements results on the longer end of the distribution determined previously [19], but is too large by a factor of 2.5. This discrepancy can be explained if the polarisability according to Fixman has the right dependence on length, but is too small by a factor of approximately 2.5. (The Mandel-Manning theory of polarisability [28] was found to give a length distribution inconsistent with previous results.)

The short end of the β-lactoglobulin fibril length distribution shows an approximately linear dependence of length concentration on length. No sign of large rod-like intermediates is apparent.

Acknowledgements

We gratefully acknowledge funding from the BBSRC for SSR, and the European Commission for an IHP grant awarded to the Food Physics Group of Wageningen University for a Marie Curie Training Site Fellowship (contract HPMT-2000-00188).

Appendices

A Dynamics of anisotropic particles in a transient electric field

The interpretation of transient electric birefringence of anisotropic particles in terms of orientation and relaxation was developed by Benoît [35,36] and O'Konski and Zimm [37], and has remained in constant use, yet essentially unchanged for the past 50 years. The orientational distribution $f(\theta, \phi, L, t)$, of particles of length L, having a rotational diffusivity $D_r(L)$, obeys the equation of motion:

$$\nabla^2 f + \frac{1}{k_B T} \nabla.(f \nabla w) = \frac{1}{D_r} \frac{\partial f}{\partial t}\,, \tag{13}$$

where k_B is Boltzman's constant, T is the absolute temperature, θ and ϕ are spherical polar coordinates set up so that the electric field E is in the direction $\theta = 0$, and t is time. w is the potential energy of the particle:

$$\nabla w = -(\Delta\alpha E^2 cos\theta - \mu E)\mathbf{e}_\theta\,, \tag{14}$$

where $\Delta\alpha(L)$ and $\mu(L)$ are the anisotropy of polarisability and the permanent dipole moment of the particle respectively, and $\mathbf{e}_\theta$ is the unit vector in the θ direction. The problem is thus rotationally symmetric in ϕ, and $f(\theta, \phi, L, t)$ can be replaced with $f'(\theta, L, t)$.

For light propagating perpendicular to the field, the birefringence Δn is given by:

$$\Delta n = M \int_0^\infty c_L(L) S(L) dL\,, \tag{15}$$

where M is the optical anisotropy per unit length concentration, and $S(L)$ is the alignment parameter of the fibrils with length L, defined as:

$$S(L, t) \equiv \frac{5}{2} \int P_2(\theta) f'(\theta, L, t)\ \sin\theta d\theta \tag{16}$$

where $P_2(\theta) = (3cos^2\theta - 1)/2$.

Since relaxation times in our system were long, in order to avoid heating and electrode effects we were forced to apply electric field pulses for times much shorter than would be required to reach a steady value of Δn. The initial linear rise of the birefringence can be calculated from Eqs. 13–16:

$$\Delta\dot{n}_{\rm init} = \frac{2ME^2}{k_B T} \int_0^\infty c_L \Delta\alpha D_r dL\,. \tag{17}$$

This gives a proportionality to E^2 analogous to the Kerr law, but applying to the initial rise rather than the steady state at long times. Note that the initial rise of birefringence does not depend on μ, the permanent dipole moment. This can be explained simply: at the start of the pulse, the fibril orientational distribution is isotropic. The field puts a torque on all the fibrils due to their permanent dipole moment, but for every fibril pointing in a direction θ, there is another pointing in a direction $\theta + \pi$ which receives an equal but opposite torque. Of the pair, one is pushed towards alignment, and the other away from alignment, and the net contribution to the birefringence is zero.

To analyse the birefringence decays, we apply a short pulse of duration Δt, after which the electric field returns to zero. It is not the purpose of this article to determine μ, and therefore we can avoid complications in the analysis due to an unknown μ by making our pulse as short as possible. For all contributions to the birefringence which diffuse slower than Δt, this ensures that the birefringence rise during the pulse is independent of μ and follows Eq. 17. For contributions which relax faster, i.e. those of the shorter length fibrils, there will be an error due to the unknown μ which can be quantified (Section 4.3).

After the pulse, the birefringence decays according to:

$$\Delta n(t) = M \int_0^\infty c_L S(L, \Delta t) e^{-6D_r t} dL\,, \tag{18}$$

which is a Laplace transformation of the length distribution, weighted by the alignment $S(L, \Delta t)$ at the end of the pulse, as a function of length. Using this equation, the measured $\Delta n(t)$ can be inverted to find c_L (Appendix B).

$S(L, \Delta t)$ can be calculated from Eqs. 13–16. Benoît expanded f' in the first three Legendre polynomials, which is a valid approximation when $\Delta\alpha E^2/k_B T$ and $\mu E/k_B T$

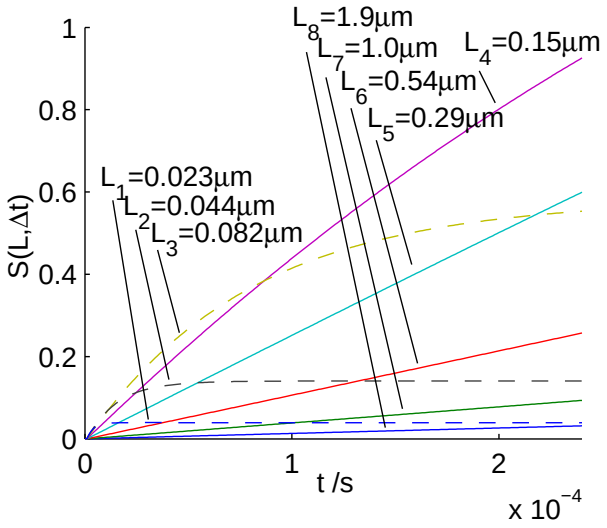

Fig. 10. Example calculations of $S(L,t)$ with a Runge-Kutta method for the sampled range of lengths, using $\Delta\alpha$ according to Fixman's theory, and taking $\mu = 0$.

are small. This is not generally true in our case, so we calculate $S(L,\Delta t)$ numerically using a Runge-Kutta method. Fig. 10 shows example calculations of $S(L,t)$ for the sampled range of lengths, using $\Delta\alpha$ according to Fixman's theory, and taking $\mu = 0$. It can be seen that S increases linearly for large L, but quickly reaches a steady state for small L.

B Inverse Laplace transform analysis

The decay curve is transformed into a spectrum of relaxation times with the following method, following Ch. 18.5 in Ref. [54]. The method is equivalent to that used in the popular program CONTIN [55]. First a solution is made by first order linear regularisation, solving the following equation by LU decomposition (see Ch. 2.3 in Ref. [54]):

$$\sum_j \left(\sum_i e^{-(\tau_k^{-1}+\tau_j^{-1})t_i} + \lambda H_{kj} \right) G_j = \sum_i e^{-t_i/\tau_k} \Delta n(t_i)\,, \tag{19}$$

which is a set of N equations in N unknowns, where G_j is the discrete contribution to the birefringence decay $\Delta n(t)$, with a decay time of τ_j, $H_{kj} = \sum_h B_{kh} B_{hj}$, where B_{hj} is the first difference matrix:

$$B_{hj} = \frac{\delta_{h,j-1} - \delta_{h,j}}{\sqrt{\tau_{h+1} - \tau_h}}\,, \tag{20}$$

and

$$\lambda = \frac{1}{N} \sum_{ij} e^{-2t_i/\tau_j}\,, \tag{21}$$

where $j,k = 1,2,3...N$ and $h = 1,2,3...(N-1)$. Second we apply the regularising condition that $G_j \geq 0$ by using the iterative equation:

$$G_k^{(p+1)} = \left| G_k^{(p)} - \epsilon \sum_j \left(\sum_i e^{-(\tau_k^{-1}+\tau_j^{-1})t_i} + \lambda H_{kj} \right) G_j^{(p)} + \epsilon \sum_i e^{-t_i/\tau_k} \Delta n_i \right|\,, \tag{22}$$

where we take the small adjustment parameter,

$$\epsilon = 2/\text{max eigenvalue}(\sum_i e^{-(\tau_k^{-1}+\tau_j^{-1})t_i} + \lambda H_{kj})\,. \tag{23}$$

1000 iterations were enough to fit the curve within the noise.

In order to estimate the fitting error due to noise, we can adjust the result of Eq. 19 before applying Eq. 22 so that we fit the curve starting from estimates biased in the positive and negative directions of s. This was done by adjusting $G_j \rightarrow G_{j+n}$ for $n = -2, -1, +1, +2$. G_j is related to the continuous distribution g by:

$$G_j = Mg\Delta L_j\,, \tag{24}$$

where ΔL_j is the sampling interval, corresponding to τ_j via the diffusion relation (Eq. 4).

C Symbols List

Here we list the symbols appearing in this paper, excluding those appearing only in the appendices. In order of appearence: Δn birefringence magnitude, t time, E electric field, Δt pulse duration, $\Delta\alpha$ anisotropy of electric polarisability of a fibril, D_r rotational diffusivity of a fibril, c_L length concentration of fibrils, L fibril length, ν dilution, M optical anisotropy of fibrils, G_j magnitude of discrete exponential component of birefringence decay curve, τ decay time, L^* entanglement length, η solvent viscosity, d diameter of fibril, g continuous interpolation of G_j, S alignment parameter, ϕ fraction of condensed counterions, z valence of counterions, b mean spacing of charges on polyelectrolyte rod, Q Bjerrum length, κ^{-1} Debye length, I molar ionic strength, γ^{-1} screening length of Fixman theory, K numerical factor in Fixman theory, z_1, z_2 valences of counter- and co-ions, c_1 concentration of counterions, μ dipole moment of a fibril, μ' dipole moment of a fibril per unit length.

References

1. J. W. Kelly, Curr. Opin. Struct. Biol **8** (1998), 101.

2. C. M. Dobson, Phil. Trans. R. Soc. Lond. B **356** (2001), 133.
3. J. A. Hardy, G. A. Higgins, Science **256** (1992), 184.
4. M. Bucciantini, E. Giannoni, F. Chiti, F. Baroni, L. Formigli, J. Zurdo, N. Taffei, G. Ramponi, C. M. Dobson, M. Stefani, Nature **416** (2002), 507.
5. C. E. MacPhee, C. M. Dobson, J. Amer. Chem. Soc. **122** (2000), 12707.
6. C. Veerman, H. Baptist, L. M. C. Sagis, van der Linden E., J. Agric. Food Chem. **51** (2003), 3880.
7. S. E. Radford, C. M. Dobson, Cell **97** (1999), 291.
8. M. R. H. Krebs, E. H. C. Bromley, S. S. Rogers, A. M. Donald, Biophys. J. **88** (2005), 2013.
9. C. M. Dobson, Methods **34** (2004), 4.
10. J. C. Rochet, P. T. Lansbury Jr, Curr. Opin. Struct. Biol **10** (2000), 60.
11. N. P. Cheremisinoff, *Handbook of polymer science and technology. Vol. 1: Synthesis and properties* (Dekker, 1989).
12. H. Kramer, M. Deggelmann, C. Graf, M. Hagenbtichle, C. Johner, R. Weber, Macromolecules **25** (1992), 4325.
13. V. J. Morris, A. R. Foweraker, B. R. Jennings, Advances in Molecular Relaxation and Interaction Processes **12** (1978), 211.
14. J. G. Elias, D. Eden, Macromolecules **14** (1981), 410.
15. J. Newman, H. L. Swinney, Biopolymers **15** (1976), 301.
16. F. Mantegazza, T. Bellini, M. Buscaglia, V. Degiorgio, D. A. Saville, J. Chem. Phys. **113** (2000), 6984.
17. B. M. I. van der Zande, G. J. M. Koper, H. N. W. Lekkerkerker, J. Phys. Chem. B **103** (1999), 5754.
18. P. A. Cirkel, G. J. M. Koper, Langmuir **14** (1998), 7095.
19. S. S. Rogers, P. Venema, L. M. C. Sagis, E. van der Linden, A. M. Donald, Macromolecules **38** (2005), 2948.
20. W. S. Gosal, A. H. Clark, P. D. A. Pudney, S. B. Ross-Murphy, Langmuir **18** (2002), 7174.
21. E. H. C. Bromley, M. R. H. Krebs, A. M. Donald, Faraday Discuss. **128** (2005).
22. L. N. Arnaudov, R. de Vries, H. Ippel, C. P. M. van Mierlo, Biomacromolecules **4** (2003), 1614.
23. L. M. C. Sagis, C. Veerman, E. van der Linden, Langmuir **20** (2004), 924.
24. P. Aymard, T. Nicolai, D. Durrand, Macromolecules **32** (1999), 2542.
25. R. K. Cannan, A. H. Palmer, A. C. Kibrick, J. Biol. Chem. **142** (1941), 803.
26. M. Mandel, Mol. Phys. **4** (1961), 489.
27. F. Oosawa, Biopolymers **9** (1970), 677.
28. G. S. Manning, Biophys. Chem. **9** (1978), 65.
29. M. Fixman, Macromolecules **13** (1980), 711.
30. G. S. Manning, J. Chem. Phys. **90** (1989), 5704.
31. M. Mandel, T. Odijk, Annu. Rev. Phys. Chem **35** (1984), 75.
32. U. Mohanty, Y. Zhao, Biopolymers **38** (1996), 377.
33. E. Fredericq, C. Houssier, *Electric Dichroism and Electric Birefringence* (Oxford University Press, 1973).
34. M. Tricot, C. Houssier, Macromolecules **15** (1982), 854.
35. H. Benoît, Compte Rendus Acad. Sci. Paris **228** (1949), 1716.
36. H. Benoît, Annales de Physique **6** (1951), 561.
37. C. T. O'Konski, B. H. Zimm, Science **111** (1950), 113.
38. M. Doi, S. F. Edwards, *Polymer Dynamics* (Oxford University Press, 1986).
39. R. Pecora, M. A. Tracy, Annu. Rev. Phys. Chem. **43** (1992), 525.
40. J. Riseman, J. G. Kirkwood, J. Chem. Phys. **18** (1950), 512.
41. J. G. Kirkwood, P. L. Auer, J. Chem. Phys. **19** (1951), 281.
42. S. Broersma, J. Chem. Phys **32** (1960), 1626.
43. M. M. Tirado, G. de la Torre, J. Chem. Phys. **73** (1980), 1986.
44. M. A. Tracy, R. Pecora, Macromolecules **25** (1992), 337.
45. K. M. Zero, R. Pecora, Macromolecules **15** (1982), 87.
46. C. Holm, M. Rehahn, W. Oppermann, M. Ballauff, Adv. Polym. Sci. **166** (2004), 1.
47. D. J. Winzor, Analytical Biochemistry **325** (2004), 1.
48. C. E. Felder, S. A. Botti, L. Lifson, I. Silman, J. L. Sussman, Journal of Molecular Graphics and Modelling **15** (1997), 318.
49. J. D. Ferry, J. L. Oncley, J. Am. Chem. Soc. **63** (1941), 272.
50. S. Brownlow, J. H. M. Cabral, R. Cooper, D. R. Flower, S. J. Yewdall, I. Polikarpov, A. C. T. North, L. Sawyer, Structure **5** (1997), 481.
51. D. Hamada, C. M. Dobson, Protein Sci. **11** (2002), 2417.
52. D. M. Walsh, D. M. Hartley, Y. Kusumoto, Y. Fezoui, M. M. Condron, A. Lomakin, G. B. Benedek, D. J. Selkoe, D. B. Teplow, J. Biol. Chem. **274** (1999), 25945.
53. H. A. Lashuel, D. M. Hartley, B. M. Petre, J. S. Wall, M. N. Simon, T. Walz, P. T. Lansbury, J. Mol. Biol. **332** (2003), 795.
54. W. H. Press, B. P. Flannery, S. A. Teukolsky, W. T. Vetterling, *Numerical Recipes in C, 2nd Ed.* (Cambridge University Press, 1993).
55. S. W. Provencher, Comput. Phys. Commun. **27** (1982), 229.